Available online at www.sciencedirect.com
ScienceDirect
Trans. Nonferrous Met. Soc. China 32(2022) 2370−2378
Transactions of Nonferrous Metals Society of China
www.tnmsc.cn

Adsorption behavior of heptyl xanthate on surface of ZnO and Cu(II) activated ZnO using continuous online in situ ATR-FTIR technology

Qi SHEN[1], Yun-hui ZHANG[1], Ying-ju FAN[1], Zheng-he XU[2], Zhong-Xi SUN[1]

1. School of Chemistry and Chemical Engineering, University of Jinan, Jinan 250022, China;
2. Department of Materials Science and Engineering,
Southern University of Science and Technology, Shenzhen 518055, China

Received 19 May 2021; accepted 10 January 2022

Abstract: A continuous online in situ attenuated total reflection Fourier-transform infrared (ATR-FTIR) spectroscopic technique was used to investigate the adsorption and desorption kinetics of heptyl xanthate (KHX) on the surface of ZnO and Cu(II) activated ZnO. The results showed that Cu(II) facilitated the xanthate adsorption process on the surface, and led to the formation of cuprous xanthate (CuX), dixanthogen (X_2) and xanthate aggregates. The adsorption of xanthate on the surface of ZnO and Cu(II) activated ZnO was found to both follow the pseudo-first-order kinetic model. When the NaOH solution was used as a desorption agent, the adsorbed xanthate can largely be removed due to the competition between OH^- and HX^-. However, for Cu(II) activated ZnO, the peak intensities at 1197 and 1082 cm^{-1} had no obvious weakening, and the absorption intensities at 1261 and 1026 cm^{-1} increased in the first 5 min, indicating an ion-exchange reaction between OH^- and surface zinc bonded xanthate HX^- and the reorganization of adsorbed xanthate.
Key words: ZnO; Cu(II) activation; continuous online in situ ATR-FTIR; heptyl xanthate; adsorption kinetics

1 Introduction

ZnO and ZnS, as two typical semiconductor materials, have been extensively applied in optoelectronics, sensor devices, dye sensitized solar cells and photocatalysts due to their distinctive properties [1−4]. Compared to the pristine ZnO, the combination of ZnO with metal sulfide (MS) may further improve the property, resulting in the development of advanced materials. Therefore, the synthesis of different core/shell structures of ZnO/ZnS has become a research focus in recent years [5−8]. To achieve the core/shell structure of metal oxide and metal sulfide, one important criterion is that the shell should have a solubility not lower than that of the core, otherwise the lower soluble product of the shell will appear with the dissolution of the core counterpart. It is well known that the solubility product(K_{sp}) of ZnO (K_{sp}=~10^{-17}) is much higher than that of ZnS (K_{sp}=~10^{-24}) [9,10], which will lead to the dissolution of ZnO along with the formation of ZnS by adding sulfide ions (HS^-) into the suspension of ZnO. Therefore, it is crucial to avoid the dissolution of ZnO when selecting the suitable sulfide source.

Alkyl xanthate is a type of widely used collector in sulfide mineral flotation, and may be an ideal candidate as a sulfide source [11]. Due to the high affinity of sulfur-containing head group to heavy metals, alkyl xanthate has been used as a collector not only for the flotation of zinc sulfide ores but also for zinc oxide ores [12,13]. The collecting ability of alkyl xanthate can be enhanced with increasing carbon chains, especially for metal oxides [14−18]. Additionally, before the xanthate

Corresponding author: Qi SHEN, E-mail: chm_shenq@ujn.edu.cn; Zhong-xi SUN, E-mail: chm_sunzx@ujn.edu.cn
DOI: 10.1016/S1003-6326(22)65953-3

adsorption on ZnO surfaces, adding other heavy metal ions, such as Cu^{2+} or Pb^{2+}, may promote the formation of ZnO@MS core/shell structure other than ZnO@ZnS. It is well known that the Cu(II) activation of sulfide minerals can enhance the adsorption rate of xanthate on their surface [19−21]. However, the adsorption of alkyl xanthate on Cu(II) activated ZnO has not received much attention.

Moreover, characterization of the surface-adsorbate interactions at the molecular level is of great importance to better understand the surface chemistry of minerals. Continuous online in situ attenuated total reflectance Fourier transform infrared (ATR-FTIR) spectroscopy is one of the most versatile techniques for measuring adsorption processes, which can provide the real-time adsorption kinetic information [22−25]. Furthermore, ATR-FTIR vibrational spectra can also provide information about the structure and orientation of adsorbed compounds [26−29]. However, the spectroscopic signals of mineral surfaces are normally weak due to their low surface/bulk ratios. The well crystallized sample with a large surface area was synthesized in this study to increase the surface/bulk ratio and further increase the FTIR signal/noise level.

Herein, a continuous online in situ attenuated total reflection Fourier-transform infrared (ATR-FTIR) spectroscopic technique was used and the results demonstrated that Cu(II) can significantly activate the adsorption rate of Potassium heptyl xanthate (KHX) on the surface of ZnO, resulting in strong ion exchange interaction between OH^- and surface zinc bonded xanthate and the reorganization of adsorbed xanthate. The adsorption of xanthate on the surface of ZnO and Cu(II) activated ZnO was found to follow the pseudo-first-order kinetic model. Our work may provide a new concept to understand the adsorption kinetics of ZnO mineral.

2 Experimental

2.1 Materials

Potassium heptyl xanthate ($C_5H_9OS_2K$, KHX) was synthesized with the purity higher than 99% according to RAO [30]. All chemicals are analytical grade, and high purity Milli-Q water (Millipore deionized, 18.2 MΩ·cm resistivity) was used in all experiments.

2.2 Preparation of ZnO and Cu(II) activated ZnO

In order to prepare ZnO, 14.5 g $Zn(NO_3)_2{\cdot}6H_2O$ and 17.6 g urea were dissolved in 100 mL distilled water. The mixed solution was placed in a 250 mL two-necked distillation flask and heated at up to 90 °C for 5 h before being separated by suction filtration. The final products were washed with deionized water and ethanol at least three times to remove impurities. The white precipitates of basic zinc carbonate were dried at 70 °C for about 12 h and then calcined at 600 °C for 90 min to remove carbonates. After centrifugation, Cu(II) activated ZnO particles were washed once with deionized water to remove extra Cu(II) ions. The ZnO or Cu(II) activated ZnO film was prepared by making a slurry (adding 10.0 mg ZnO or Cu(II) activated ZnO in 5 mL ethanol). The obtained slurry was put in an ultrasonic bath for 1 h, and then spread over a clean and dry ZnSe (45°) crystal and dried overnight in air at room temperature, forming a new freshly deposited film.

2.3 Continuous online in situ ATR-FTIR spectroscopic investigation

ATR-FTIR spectra were observed using an HAATR Plus accessory (Pike Technologies) installed in a Bruker VERTEX−70 FTIR spectrometer equipped with a DTGS detector. A 45° ZnSe crystal (50 mm × 10 mm × 4 mm) was mounted in a flow cell. A peristaltic pump (Model BT300L) with Tygon LFL tubing was used to pump KHX solution (1.0 mmol/L) from the beaker to the ATR-cell at a rate of 3 mL/min. The collected background spectrum consisted of the absorbance of the ZnSe crystal and deposited mineral film. Each ATR-FTIR spectrum was collected at a resolution of 4 cm^{-1} with 100 scans. The original measured wavenumber range was within 4000−800 cm^{-1}. All the original spectra were baseline corrected and all the measurements were performed at room temperature.

2.4 Desorption experiments

Deionized water was added through the flow cell until no variation in the spectra could be detected, and then the background scans were run. The collection of adsorption spectra started as soon as the KHX solution entered the ATR flow cell. The desorption experiments began after the adsorption

experiments were finished using deionized water or 0.01 mol/L NaOH solution as desorbents. The collection of desorption spectra started as soon as the desorbent entered the ATR-FTIR flow cell and was recorded for 30 min. The residual concentration of xanthate was measured using a UV-Vis spectrophotometer at the wavelength of 301 nm.

3 Results and discussion

3.1 ATR-FTIR spectroscopic analysis

As shown in Figs. 1(a, b), the crystal structure of basic zinc carbonate and final ZnO was confirmed by the X-ray powder diffraction (XRD), which corresponds to JCPDS cards of $Zn_4CO_3(OH)_6$ (No. 11-0287) and ZnO (No. 36-1451), respectively. The surface area of ZnO sample was measured to be 13 m^2/g using BET method. In order to prepare the Cu(II) activated ZnO sample, 10.0 mg of synthesized ZnO sample was added in 25 mL pure water or cupric nitrate (0.5 mmol/L) solution for 2 h. To investigate the adsorption behavior of xanthate on the surface of ZnO and Cu(II) activated ZnO, a continuous online in situ attenuated total reflection Fourier-transform infrared (ATR-FTIR) spectroscopic technique was used and the experimental arrangement is shown in Fig. 2.

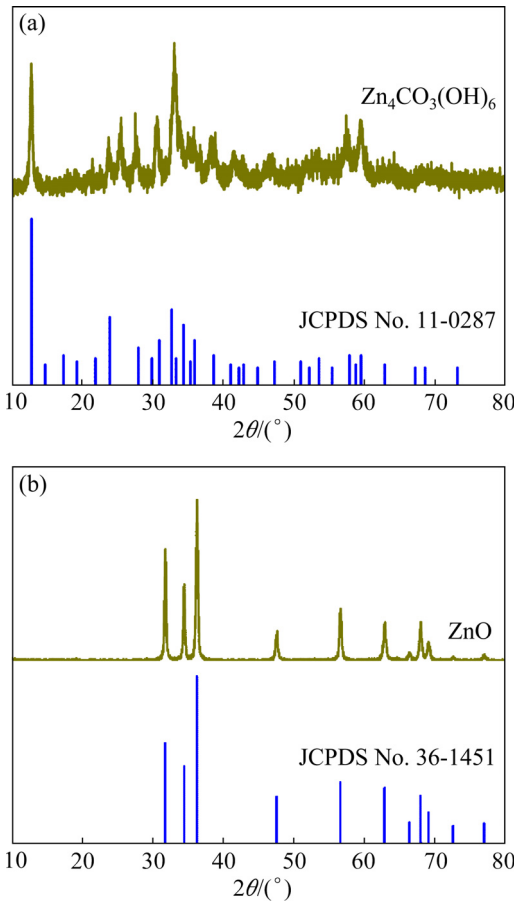

Fig. 1 XRD results of basic zinc carbonate (a) and synthesized ZnO (b)

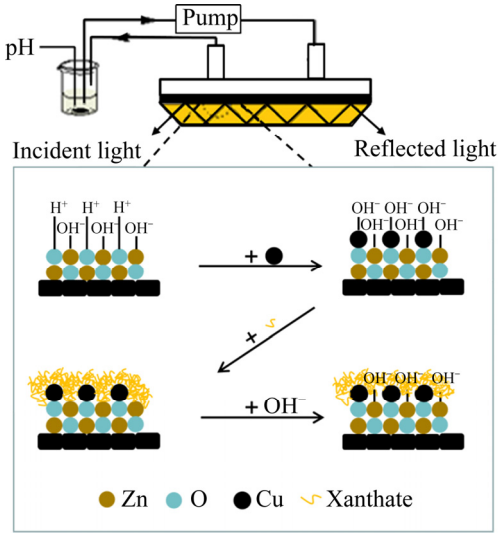

Fig. 2 Continuous online in situ ATR-FTIR device

FTIR spectra in 1500−950 cm^{-1} region were specially examined, where most important vibrations of the xanthate functional groups were observed. Figures 3(a, b) show the region of adsorbed KHX on the surface of ZnO and Cu(II) activated ZnO, respectively, and evidently revealed that the peak intensity was enhanced with the increase of time for both samples. Although the FTIR spectra of two samples were largely similar, some differences in peak positions were clear. The FTIR spectra absorbance peaks for ZnO sample located at 1463, 1377, 1207, 1143, 1085 and 1045 cm^{-1}, respectively. Marginal peaks located at about 1426, 1265 and 1000 cm^{-1} can also be observed. Some shoulders became visible at 1197, 1133 and 1028 cm^{-1}. FTIR peaks for Cu(II) activated ZnO sample, the FTIR peaks showed up at 1463, 1379, 1260 and 1198, 1144, 1128, 1082 and 1026 cm^{-1} correspondingly and the shoulders turned up at 1248 and 1046 cm^{-1}.

In order to distinguish the overlapped peaks in the 1300−950 cm^{-1} range, Gaussian function was used to closely analyze the spectra as presented in Fig. 4. For ZnO sample, the FTIR bands at 1207 and 1045 cm^{-1} can be resolved into two peaks at 1210 and 1197 cm^{-1}, and at 1050 and 1028 cm^{-1}, respectively. For Cu(II) activated ZnO sample, the FTIR spectra bands at 1260 and 1026 cm^{-1} can

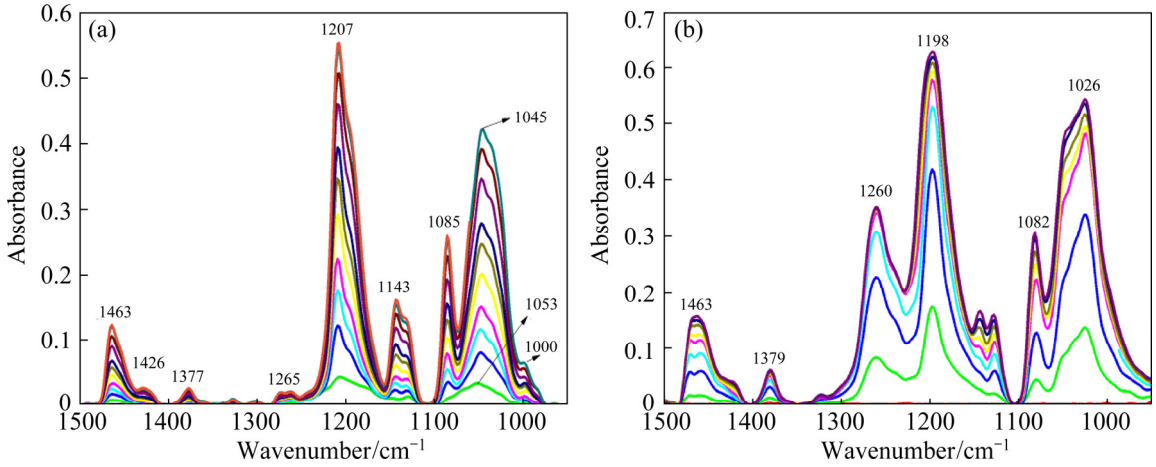

Fig. 3 FTIR spectra of KHX adsorbed on surface of ZnO (a), and Cu(II) activated ZnO (b) ((a) 0, 10, 20, 30, 40, 60, 80, 100, 140, 180, 210 and 220 min from bottom to up; (b) 0, 10, 20, 30, 50, 70, 90, 110 and 120 min from bottom to up)

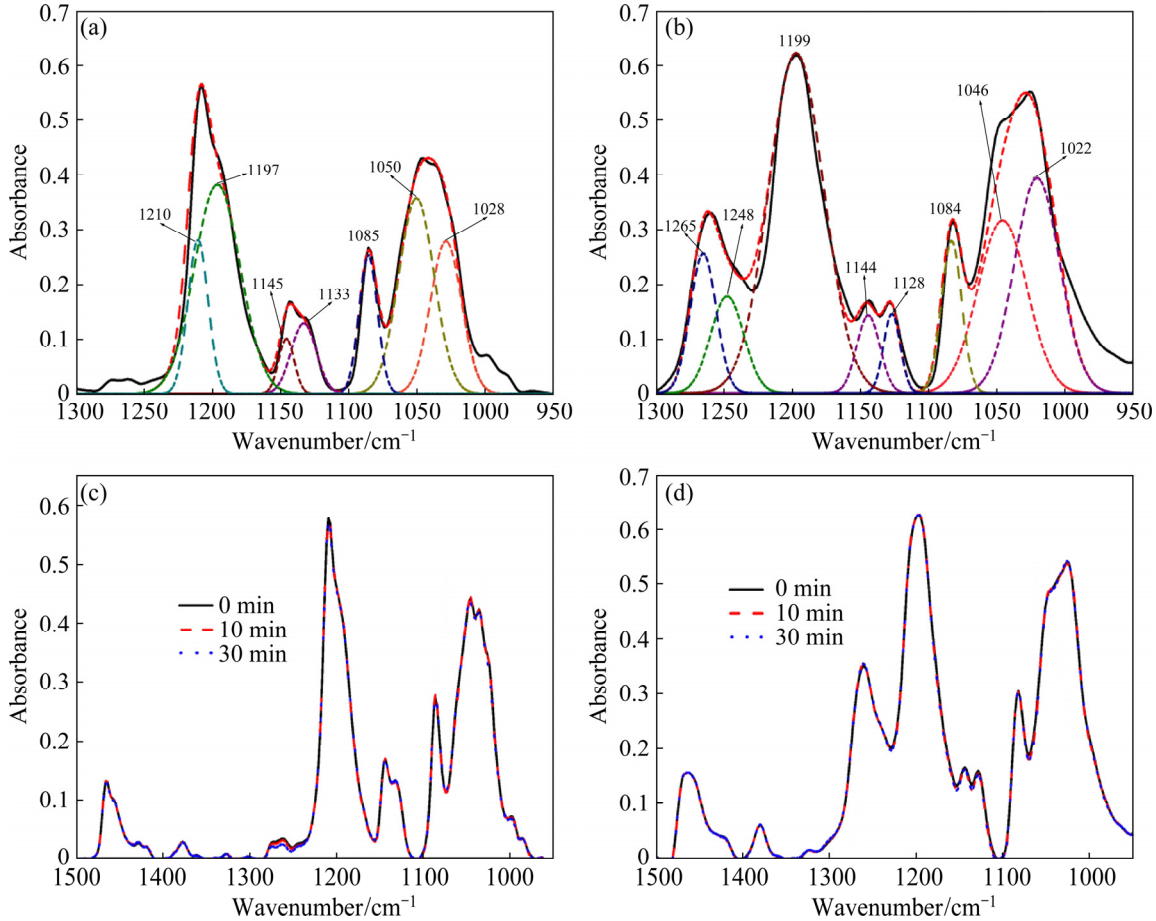

Fig. 4 Curve-fitting results for representative spectra collected from 1300 to 950 cm^{-1} for KHX adsorbed on surface of ZnO at 220 min (a) and Cu(II) activated ZnO at 120 min (b), and ATR-FTIR spectra collected as function of time for ZnO (c) and Cu(II) activated ZnO (d) using pure water as desorption agent

be resolved into two peaks at 1265 and 1248 cm^{-1}, and at 1046 and 1022 cm^{-1}, respectively. This region of FTIR spectra (1300−950 cm^{-1}) is mainly contributed to the CS_2, C — O — C vibrations together with wagging, twisting and rocking of the CH_3/CH_2 entities in the heptyl chain [31−33]. The assignments for main FTIR spectra absorbance peaks from two samples are listed in Table 1 with logical adaption to KHX−ZnO and KHX−Cu(II)−ZnO systems. The main difference of FTIR spectra

Table 1 FTIR adsorbance peak positions and intensities in KHX−ZnO and KHX−Cu(II)−ZnO systems and their assignments [34−36]

Wavenumber/ cm^{-1}	Intensity	Assignment
1463[a,b]	0.154[b], 0.120[a]	—CH_3— asym def, —CH_2— sym def
1379[b]	0.06	—CH_3— sym def, —CH_2— waging stretch
1377[a]	0.025	—CH_3— sym def, —CH_2— waging stretch
1265[b]	0.255	C—O—C/S—C—S asym stretch —CH_2— twist stretch
1248[b]	0.177	C—O—C asym stretch S—C—S sym stretch, —CH_2— twist stretch
1210[a]	0.279	C—O—C bend stretch
1199[b]	0.622	C—O—C asym stretch, —CH_2— waging stretch, C—O—C out-of-plane bend stretch
1197[a]	0.383	C—O—C asym stretch
1145[a]	0.100	C—O—C asym stretch
1144[b]	0.142	C—O—C asym stretch
1133[a]	0.128	C—C—C/C—O—C/O—C—C def S—C—S asym stretch
1128[b]	0.145	S—C—S asym stretch
1085[a]	0.253	C—O—C stretch, C—C—C/C—O—C def, S—C—S asym stretch
1084[b]	0.280	C—O—C stretch, C—C—C/C—O—C def, S—C—S asym stretch
1050[a]	0.356	S—C—S asym stretch
1046[b]	0.317	—CH_2— waging stretch, S—C—S asym stretch
1028[a]	0.278	S—C—S asym stretch
1022[b]	0.395	C—C—C stretch, C—C—C def, C—O—C stretch, S—C—S asym stretch
1000[a]	0.064	C—C—C stretch, C—C—C def, C—O—C stretch, S—C—S asym stretch

[a]: KHX−ZnO; [b]: KHX−Cu(II)−ZnO; asym def: asymmetric deformation; sym def: symmetric deformation; asym stretch: asymmetric stretch; sym stretch: symmetric stretch; def: deformation

from copper xanthate and zinc xanthate interactions was different peak positions at 1265 cm^{-1} (Fig. 4(a)) and 1026 cm^{-1} (Fig. 4(b)) attributed to COC/CS_2 asymmetric stretching and CH_2 twist vibrations from dixanthogen, respectively, besides a few wave number red shifts of peaks for Cu(II) activated ZnO. As shown in Fig. 4, the spectrum of adsorbed KHX showed typical peaks at around 1265 cm^{-1} due to the formation of X_2 and at 1022 cm^{-1}, indicating that Cu^{2+} could readily react with HX^- to promote the formation of dixanthogen. The same phenomena were observed for adsorption of butyl xanthate on the surface of CuO in our previous study [37].

The adsorption of xanthate on the surface of ZnO and Cu(II) activated ZnO was found to be far above the monolayer adsorption by the calculation of the adsorption capacity of xanthate on the sample surfaces. The area occupied by a xanthate molecule is about 0.4 nm^2, thus the monolayer capacity for xanthate on a mineral surface is about 2.5 nm^{-2}. According to the adsorption data in this study, the adsorption densities of xanthate at ZnO and Cu(II) activated ZnO were as high as 224 and 266 mg/g, respectively, which is far above the monolayer density. According to the FTIR spectra, it is assumed that the surface xanthate aggregates or surface micelle were formed and enhanced during the adsorption process. Figure 4 shows that the appearance of FTIR spectra at 1197 and 1028 cm^{-1} from xanthate on ZnO surface may be attributed to the existence of surface aggregates. In addition, the formation of dixanthogen indicates that the xanthate may be oxidized. However, in this case, the concentration of oxidant (Cu(II)) was far less than that of xanthate, and therefore the FTIR spectrum at 1265 cm^{-1} may be induced not only by dixanthogen but also by the surface aggregates. Figures 4(c) and (d) show the FTIR spectra of KHX xanthate after being rinsed with water. The absorbance intensity had no obvious changes, indicating that xanthate was chemisorbed on the sample surface.

The results of xanthate desorption using a 0.01 mol/L NaOH solution are presented in Fig. 5. In Fig. 5(a), the absorption intensity decreased dramatically in the first 10 min, confirming the competition between OH^- and HX^- and the replacement of surface xanthate sites by OH^-. According to the FTIR absorbance intensity, the desorption efficiency of xanthate on the surface of ZnO after being rinsed with NaOH solution was calculated to be about 94%, indicating that OH^- replaced most of xanthates on the surface of ZnO. It

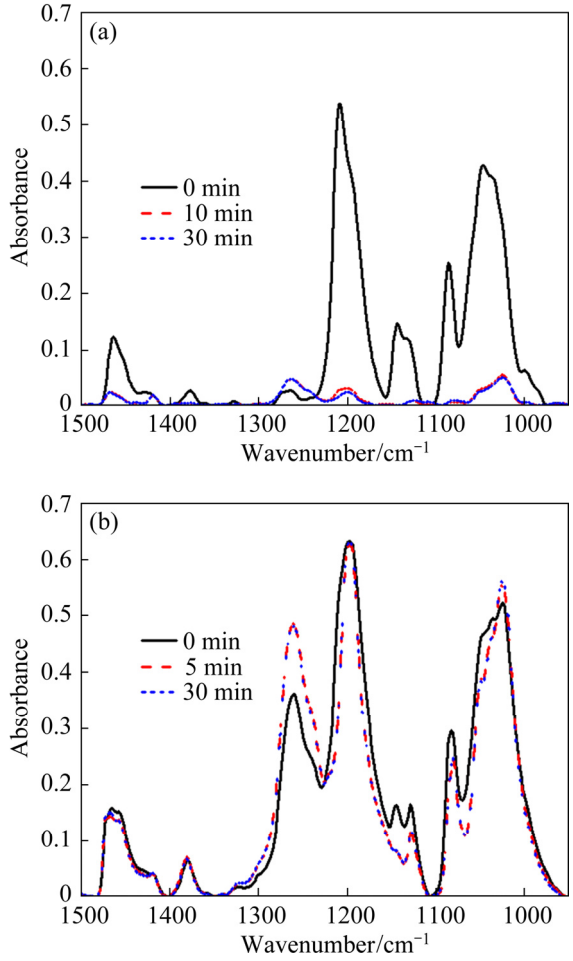

Fig. 5 ATR-FTIR absorption spectra collected as function of time using diluted NaOH solution as desorption agent: (a) ZnO; (b) Cu(II) activated ZnO

is worth noting that after desorption with OH^-, 6% xanthate still remained on the surface. According to the adsorption density of xanthate on ZnO sample, the percentage of removed xanthate was calculated as 94.2%, corresponding to a monolayer (2.5 nm^{-2} is the theoretical monolayer density of xanthate on a mineral surface). However, as for Cu(II) activated ZnO, the FTIR intensity of xanthate showed no change, indicating the higher affinity of Cu(I) with HX^- than with OH^- as described in Eq. (1):

$$\equiv OZnX_n^{(n-1)-}+OH^-\rightarrow\equiv OZnXOH^-+(n-1)X^- \quad (1)$$

where $\equiv$OZnX is xanthate site on the surface of ZnO, and X^- is heptyl xanthate.

As shown in Fig. 5(b), the absorbance intensity of FTIR spectra at 1261 and 1026 cm^{-1} increased in the first 5 min, and then became constant. At the same time, the peak intensities at 1199 and 1082 cm^{-1} slightly declined. These observations implied that during the desorption process of xanthate from Cu(II) activated ZnO, OH^- did not replace adsorbed xanthate but promoted its reorganization. Meanwhile, OH^- ions only replaced a small portion of the HX^- sites on the surface. This process is visualized in Fig. 2. The surface chemical reactions in this process are summarized as

$$\equiv OZnOH+Cu(II)^+\rightarrow\equiv OZnOCu(II)^++H^+ \quad (2)$$

$$\equiv OZnOCu(II)^++nX^-\rightarrow\equiv OZnOCu(I)X_n^{(n-1)-} \quad (3)$$

$$\equiv OZnOCu(I)X_n^{(n-1)-}+OH^-\rightarrow \equiv OZnOCu(I)OHX_n^{(n-1)-} \quad (4)$$

3.2 Adsorption kinetics

Our previous study confirmed that the adsorption of xanthate on clean ZnSe crystal was negligible [37−39]. The ATR-FTIR absorbance intensity at 1200 cm^{-1} was used to generate kinetic curves. The adsorption/desorption curves for ZnO and Cu(II) activated ZnO are shown in Fig. 6(a). It was shown that the FTIR absorbance intensity of adsorbed KHX increased rapidly at the beginning, then increased slowly, and eventually reached equilibrium. In comparison with the adsorption/desorption curves of ZnO and Cu(II) activated ZnO, the adsorption rate of KHX was significantly enhanced for the Cu(II) activated ZnO sample, which is consistent with earlier findings [39,40]. The adsorption capacity in this study was calculated according to the following formula:

$$q_e=\frac{(c_0-c_1)VM}{m} \quad (5)$$

where c_0 is the initial concentration of xanthate, c_0=1.0 mmol/L; c_1 is the adsorption equilibrium concentration of xanthate, c_1=0.9610 mmol/L (ZnO) or 0.9537 mmol/L (Cu(II) activated ZnO); V is the total volume of xanthate solution, V=250 mL; M is the molar mass of heptyl xanthate, M=230 g/mol; m is the total mass of ZnO or Cu(II) activated ZnO, m=0.01 g. The adsorption capacities of ZnO and Cu(II) activated ZnO were calculated as 224 and 266 mg/g with corresponding adsorption densities of 45 nm^{-2} and 54 nm^{-2}, respectively. With some differences in adsorption capacities of xanthate on ZnO and Cu(II) activated ZnO, the adsorption rate on Cu(II) activated ZnO was significantly high with a sharp slope. In order to investigate the adsorption kinetics of KHX onto the surface of ZnO and Cu(II) activated ZnO, the pseudo first-order model (Eq. (6)) and pseudo second-order model (Eq. (7)) were used

to fit the experimental data. The time required to uptake half of the amount adsorbed at equilibrium, $t_{0.5}$, is typically considered as a measure of the rate of adsorption and can be calculated by Eqs. (8) and (9) for the pseudo first-order model and pseudo second order model, respectively, which is typically considered as a measure of the rate of adsorption.

$$q_t = q_e[1-\exp(-k_1 t)] \tag{6}$$

$$q_t = \frac{q_e^2 k_2 t}{1+q_e k_2 t} \tag{7}$$

$$t_{0.5} = \frac{\ln 0.5}{-k_1} \tag{8}$$

$$t_{0.5} = \frac{1}{k_2 q_e} \tag{9}$$

where q_e (mg/g) was the adsorbed amount of xanthate at equilibrium, q_t (mg/g) was the adsorbed amount at time t (min), and k_1 (min^{-1}) and k_2 (g·mg^{-1}·min^{-1}) were rate constants. Figure 6(b) shows the fitting of the pseudo first-order and pseudo second-order models for the KHX adsorption on the surface of ZnO and Cu(II) activated ZnO with their model parameters listed in Table 2. Obviously, both kinetic models show a good fit to the adsorption data (R^2>0.99), thus the simple model is preferred. As there is little difference in adsorption kinetics, we concluded that the adsorption of KHX on both ZnO and Cu(II) activated ZnO followed the pseudo first-order kinetic model due to the higher R^2 values and lower AIC values. The adsorption rate on the surface of Cu(II) activated ZnO more than doubled that for ZnO (0.034 versus 0.015), which also quantitatively explains why Cu(II) is used as a good activator for the zinc mineral flotation when alkyl xanthate is used as a collector.

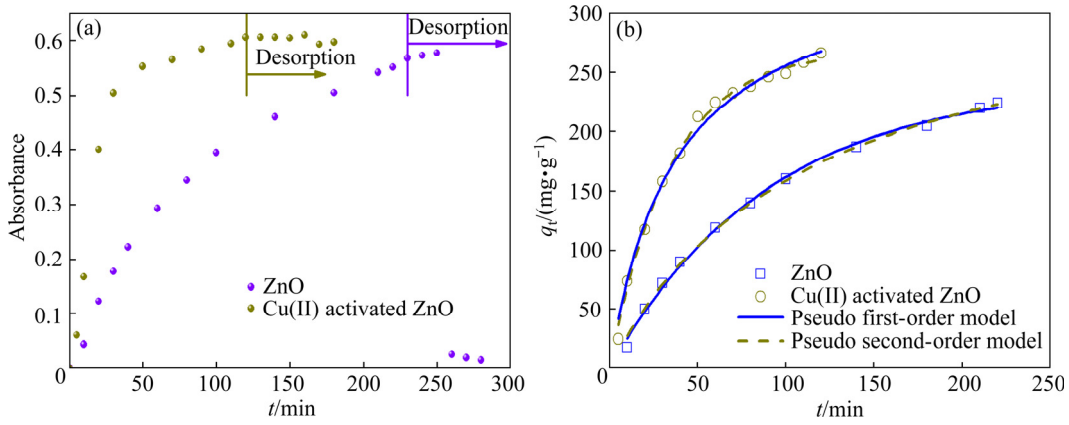

Fig. 6 Adsorption of KHX as function of time on surface of ZnO and Cu(II) activated ZnO (a), and fitting of pseudo first-order and pseudo second-order models for KHX adsorption onto surface of ZnO and Cu(II) activated ZnO (b)

Table 2 Kinetic model parameters for KHX adsorption onto ZnO and Cu(II) activated ZnO

Model	Parameter	ZnO	Cu(II) activated ZnO
Pseudo first-order model	q_e/(mg·g^{-1})	241.55±4.51	267.98±3.80
	k_1/min^{-1}	(0.01±4.68)×10^{-4}	(0.03±1.25)×10^{-3}
	$t_{0.5}$/min	69.3	23.1
	R^2	0.997	0.995
	AIC	37.0	50.4
Pseudo second-order model	q_e/(mg·g^{-1})	338.00±8.37	349.86±11.00
	k_2/(g·mg^{-1}·min^{-1})	2.62×10^{-5}±2.03×10^{-6}	7.73×10^{-5}±9.11×10^{-6}
	$t_{0.5}$/min	112.9	37.0
	R^2	0.998	0.991
	AIC	34.4	58.2
Experimental values	q_e/(mg·g^{-1})	224	266

AIC is Akaike information criterion; R^2 is correlation coefficient

4 Conclusions

(1) Online in situ ATR-FTIR technique is a useful tool to study the adsorption kinetics of xanthate on mineral surfaces.

(2) The adsorption of KHX on the surface of ZnO and Cu(II) activated ZnO followed the pseudo first-order kinetic model.

(3) The adsorption rate of KHX on the surface of ZnO increased significantly by the Cu(II) activation.

(4) The KHX adsorption on the Cu(II) activated ZnO surface was stronger than that of OH^-, but OH^- can promote the reorganization of xanthate on the surface.

(5) The formation of xanthate aggregates on the surface of ZnO may be identified respectively by the red shifts of FTIR spectrum from the wave-number of 1200 to 1197 cm^{-1} and 1045 to 1028 cm^{-1} and the enhancement of FTIR spectrum at 1265 and 1022 cm^{-1} in the presence of Cu(II) ions.

Acknowledgments

This work is supported by the National Natural Science Foundation of China (Nos. 51274104, 50874052), and the National Basic Research Program of China (No. 2011CB933700). Dr. Teresa BISSON from University of Alberta is acknowledged for valuable comments and linguistic corrections.

References

[1] CHU H O, WANG Q, SHI Y J, SONG S G, LIU W G, ZHOU S, GIBSON D, ALAJLANI Y, LI C. Structural, optical properties and optical modelling of hydrothermal chemical growth derived ZnO nanowires [J]. Transactions of Nonferrous Metals Society of China, 2020, 30: 191−199.

[2] SUN Y Q, SUN Y G, ZHANG T, CHEN G Z, ZHANG F S, LIU D L, CAI W P, LI Y, YANG X F, LI C C. Complete Au@ZnO core-shell nanoparticles with enhanced plasmonic absorption enabling significantly improved photocatalysis [J]. Nanoscale, 2016, 8: 10774−10782.

[3] ZUBAIR N, AKHTAR K. Morphology controlled synthesis of ZnO nanoparticles for in-vitro evaluation of antibacterial activity [J]. Transactions of Nonferrous Metals Society of China, 2020, 30: 1605−1614.

[4] DU H Y, YANG W, YI W C, SUN Y H, YU N S, WANG J. Oxygen-plasma-assisted enhanced acetone-sensing properties of ZnO nanofibers by electrospinning [J]. ACS Applied Materials & Interfaces, 2020, 12: 23084−23093.

[5] TARISH S, XU Y, WANG Z J, MATE F, AL-HADDAD A, WANG W X, LEI Y. Highly efficient biosensors by using well-ordered ZnO/ZnS core/shell nanotube arrays [J]. Nanotechnology, 2017, 28: 405501.

[6] YAN H L, LI T, LU Y, CHENG J B, PENG T, XU J Y, YANG L Y, HUA X Q, LIU Y X, LUO Y S. Template-free synthesis of ordered ZnO@ZnS core-shell arrays for high performance supercapacitors [J]. Dalton Transactions, 2016, 45: 17980−17986.

[7] SERRÀ A, PHILIPPE L. Simple and scalable fabrication of hairy ZnO@ZnS core@shell Cu cables for continuous sunlight-driven photocatalytic water remediation [J]. Chemical Engineering Journal, 2020, 401: 126164.

[8] RU F, XIA J, LI X Z, WANG Y F, HUA Z, SHAO R W, WANG X C, LEE C S, MENG X M. Al_2O_3 buffer-facilitated epitaxial growth of high-quality ZnO/ZnS core/shell nanorod arrays [J]. Nanoscale, 2021, 13: 11525−11533.

[9] SUN Z X, SKÖLD R O. A multi-parameter titration method for the determination of formation pH for metal hydroxides [J]. Minerals Engineering, 2001, 14: 1429−1443.

[10] RÖNNGREN L, SJÖBERG S, SUN Z X, FORSLING W. Surface reactions in aqueous metal sulfide systems: 5. The complexation of sulfide ions at the ZnS−H_2O and PbS−H_2O interfaces [J]. Journal of Colloid and Interface Science, 1994, 162: 227−235.

[11] ZHANG Y H, WU L M, HUANG P P, SHEN Q, SUN Z X. Determination and application of the solubility product of metal xanthate in mineral flotation and heavy metal removal in wastewater treatment [J]. Minerals Engineering, 2018, 127: 67−73.

[12] BAG B, DAS B, MISHRA B K. Geometrical optimization of xanthate collectors with copper ions and their response to flotation [J]. Minerals Engineering, 2011, 24: 760−765.

[13] JIA K, FENG Q M, ZHANG G F, JI W Y, ZHANG W K, YANG B Q. The role of S(II) and Pb(II) in xanthate flotation of smithsonite: Surface properties and mechanism [J]. Applied Surface Science, 2018, 442: 92−100.

[14] FENG B, FENG Q M, LU Y P, LV P C. The effect of conditioning methods and chain length of xanthate on the flotation of a nickel ore [J]. Minerals Engineering, 2012, 39: 48−50.

[15] SOUTO R M, LAZ M M, GONZÁLEZ S. X-ray photoelectron spectroscopy and electrochemical studies on the interaction of potassium ethyl xanthate with metallic copper [J]. The Journal of Physical Chemistry B, 1997, 101: 508−511.

[16] MIELCZARSKI J A, MIELCZARSKI E, CASES J M. Influence of chain length on adsorption of xanthates on chalcopyrite [J]. International Journal of Mineral Processing, 1998, 52: 215−231.

[17] EJTEMAEI M, GHARABAGHI M, IRANNAJAD M. A review of zinc oxide mineral beneficiation using flotation method [J]. Advances in Colloid and Interface Science, 2014, 206: 68−78.

[18] NAKLICKI M L, RAO S R, GOMEZ M, FINCH J A. Flotation and surface analysis of the nickel (II) oxide/amyl xanthate system [J]. International Journal of Mineral Processing, 2002, 65: 73−82.

[19] PRESTIDGE C A, SKINNER W M, RALSTON J, SMART R S C. Copper(II) activation and cyanide deactivation of zinc sulphide under mildly alkaline conditions [J]. Applied Surface Science, 1997, 108: 333−344.

[20] ZHU Z Z, TANG X D, CEN J H, LI J X, WU W Q, JIANG H F. Copper-catalyzed synthesis of thiazol-2-yl ethers from oxime acetates and xanthates under redox-neutral conditions [J]. Chemical Communications, 2018, 54: 3767−3770.

[21] PRESTIDGE C A, THIEL A G, RALSTON J, SMART R S

C. The interaction of ethyl xanthate with copper (II)-activated zinc sulphide: Kinetic effects [J]. Colloids and Surfaces A, 1994, 85: 51−68.
[22] GE D L, FAN Y J, YIN L, SUN Z X. Determination of the adsorption of xanthate on mesoporous $CuAl_2O_4$ using a continuous online in situ ATR-FTIR technology [J]. Acta Physico-Chimica Sinica, 2013, 29: 371−376.
[23] CARABANTE I, GRAHN M, HOLMGREN A, HEDLUND J. In situ ATR-FTIR studies on the competitive adsorption of arsenate and phosphate on ferrihydrite [J]. Journal of Colloid and Interface Science, 2010, 351: 523−531.
[24] WANG Z, LARSSON M L, GRAHN M, HOLMGREN A, HEDLUND J. Zeolite coated ATR crystals for new applications in FTIR-ATR spectroscopy [J]. Chemical Communications, 2004, 24: 2888−2889.
[25] MITCHELL W, GOLDBERG S, AL-ABADLEH H A. In situ ATR-FTIR and surface complexation modeling studies on the adsorption of dimethylarsinic acid and p-arsanilic acid on iron-(oxyhydr) oxides [J]. Journal of Colloid and Interface Science, 2011, 358: 534−540.
[26] BORER P, HUG S J. Photo-redox reactions of dicarboxylates and α-hydroxydicarboxylates at the surface of Fe(III) (hydr)oxides followed with in situ ATR-FTIR spectroscopy [J]. Journal of Colloid and Interface Science, 2014, 416: 44−53.
[27] NEIVANDT D J, GEE M L, HAIR M L, TRIPP C P. Polarized infrared attenuated total reflection for the in situ determination of the orientation of surfactant adsorbed at the solid/solution interface [J]. The Journal of Physical Chemistry B, 1998, 102: 5107−5114.
[28] LARSSON M L, FREDRIKSSON A, HOLMGREN A. Direct observation of a self-assembled monolayer of heptyl xanthate at the germanium/water interface: a polarized FTIR study [J]. Journal of Colloid and Interface Science, 2004, 273: 345−349.
[29] GUO C E, GUO X M, CHU W B, JIANG N, LI H. FTIR-ATR study for adsorption of trypsin in aqueous environment on bare and TiO_2 coated ZnSe surfaces [J]. Chinese Chemical Letters, 2020, 31: 150−154.
[30] RAO S R. Xanthate and related compounds [M]. New York: Marcel Dekker, Inc., 1971.
[31] HELLSTRÖM P, ÖBERG S, FREDRIKSSON A, HOLMGREN A. A theoretical and experimental study of vibrational properties of alkyl xanthates [J]. Spectrochimica Acta Part A: Molecular and Biomolecular Spectroscopy, 2006, 65: 887−895.
[32] JANG W H, MILLER J D. Verification of the internal reflection spectroscopy adsorption density equation by Fourier transform infrared spectroscopy analysis of transferred Langmuir-Blodgett films [J]. Langmuir, 1993, 9: 3159−3165.
[33] WOODS R, HOPE G A, BROWN G M. Spectroelectrochemical investigations of the interaction of ethyl xanthate with copper, silver and gold: II. SERS of xanthate adsorbed on silver and copper surfaces [J]. Colloids and Surfaces A, 1998, 137: 329−337.
[34] LARSSON M L, HOLMGREN A, FORSLING W. Xanthate adsorbed on ZnS studied by polarized FTIR-ATR spectroscopy [J]. Langmuir, 2000, 16: 8129−8133.
[35] FREDRIKSSON A, HOLMGREN A. An in situ ATR-FTIR study of the adsorption kinetics of xanthate on germanium [J]. Colloids and Surfaces A, 2007, 302: 96−101.
[36] FREDRIKSSON A, HELLSTRÖM P, ÖBERG S, HOLMGREN A. Comparison between in situ total internal reflection vibrational spectroscopy of an adsorbed collector and spectra calculated by ab initio density functional theory methods [J]. The Journal of Physical Chemistry C, 2007, 111: 9299−9304.
[37] SHEN Q, FAN Y J, YIN L, SUN Z X. Two-dimensional continuous online in situ ATR-FTIR spectroscopic investigation of adsorption of butyl xanthate on CuO surfaces [J]. Acta Physico: Chimica Sinica, 2014, 30: 359−364.
[38] SHEN Q, FAN Y J, ZHANG W M, ZHU B L, WANG R, SUN Z X. Two-dimensional correlation analysis of continuous online in situ ATR-FTIR on the adsorption of butyl xanthate at the surface of α-PbO [J]. Chinese Chemical Letters, 2015, 26: 193−196.
[39] SHEN Q, ZHANG Y H, FAN Y J, XU Z H, SUN Z X. Two-dimensional correlation analysis of continuous online in situ ATR-FTIR on the adsorption of heptyl xanthate at the surface of ZnS and Pb(II) activated ZnS [J]. Minerals Engineering, 2019, 144: 106019.
[40] POPOV S R, VUČINIĆ D R. The ethylxanthate adsorption on copper-activated sphalerite under flotation-related conditions in alkaline media [J]. International Journal of Mineral Processing, 1990, 30: 229−244.

连续在线原位 ATR-FTIR 技术研究庚基黄药在 ZnO 和 Cu(II)活化 ZnO 表面的吸附行为

沈 琪[1]，张云惠[1]，范迎菊[1]，徐政和[2]，孙中溪[1]

1. 济南大学 化学化工学院，济南 250022；2. 南方科技大学 材料科学与工程系，深圳 518055

摘 要：采用连续在线原位衰减全反射傅里叶变换红外光谱(ATR-FTIR)技术研究庚基黄原酸盐(KHX)在合成高纯氧化锌和 Cu(II)活化氧化锌矿物表面的吸附和解吸动力学。研究结果表明，添加 Cu(II)能显著提高 KHX 在 ZnO 表面的吸附率，生成黄盐酸亚铜、双黄原和黄原酸盐聚集体。研究发现 KHX 在氧化锌和 Cu(II)活化氧化锌表面吸附符合拟一级动力学模型。由于 OH^-和 HX^-离子竞争，NaOH 水溶液作为解吸剂可基本脱出氧化锌表面吸附的 KHX。而对于 Cu(II)活化氧化锌表面，1197 和 1082 cm^{-1} 处的峰强度没有明显减弱，在 1261 和 1026 cm^{-1} 吸附强度在前 5 min 增加，表明表面吸附 HX^-和 OH^-之间的离子交换反应和表面吸附 KHX 的重组作用。

关键词：氧化锌；Cu(II)活化；连续在线原位衰减全反射傅里叶变换红外光谱；庚基黄药；吸附动力学

(Edited by Xiang-qun LI)